Structure and phase behavior of two-Yukawa fluids with competing interactions in planar slit pores

Eun-Young Kim and Soon-Chul Kim*
Department of Physics, Andong National University, Andong 760-749, Korea

Soong-Hyuck Suh†
Department of Chemical Engineering, Keimyung University, Daegu 704-701, Korea
(Received 19 January 2012; published 14 May 2012)

A density functional perturbation theory, which is based both on the modified fundamental-measure theory and on the first-order mean-spherical approximation for long-range attractive and repulsive interactions, has been developed for studying the structure and phase behaviors of a competing system restricted to slit pores. The hysteresis loop for the adsorption and desorption curves indicates that the system exhibits vapor-cluster and cluster-liquid transitions which depend on the pair potential parameters and the slit width (H). The periodic spacing (D) of the cluster is commensurate with the periodicity of modulation in the particle density distribution and more closely related to the vapor-cluster and cluster-liquid phase transitions of the system. For the cluster phase, we find the transition from a single liquidlike slab to a multi-liquidlike slab with increasing the slit width. The multi-liquidlike slab is formed depending on the periodicity of modulation by finite-size artifacts. The cluster-related phase transitions, such as the vapor-cluster or cluster-liquid transitions occur for $H > D$, while for $H < D$ the system only exhibits the vapor-liquid transition. At a low amplitude, the vapor-liquid transition disappears and the cluster-liquid transition only occurs for $H < D$. The coexistence curves for the confined phase diagram are contained within the corresponding bulk liquid-vapor coexistence curve. For a wide slit pore ($H > D$), the system exhibits two tricritical points, joined to one another by the line of second-order transition. The results support the conclusion that the confinement effect plays an important role in determining the equilibrium phase transition.

DOI: 10.1103/PhysRevE.85.051203 PACS number(s): 61.20.Gy, 82.70.−y, 64.70.pv

I. INTRODUCTION

Over the past years, considerable progress has been made in the understanding of microphase formation induced by competing interactions, which are attractive at a short distance and repulsive at a long distance [1–13]. An effective potential such as the competing interaction can be found in colloid-polymer mixtures. The interaction between the colloids may be influenced by the presence of other species, and the mixture experiences attractive and repulsive interactions, i.e., competing interactions. In a colloid-polymer mixture, the long-range repulsion arises from the colloids being charged, while the attraction at a short distance stems from the depletion forces associated with nonadsorbing polymers. Such competing interactions give rise to various microphase separated phases, including the cluster phases, because the attraction favors bulk phase separation and the repulsion disfavors it. A balance between these interaction yields finite-size mesophases. The cluster morphology depends on the ranges of the competing interactions and on the density, but also the temperature can have a role.

Many studies have been carried out to investigate the bulk phase behaviors of competing systems due to their ability to represent many real fluids in two- and three-dimensional systems [1,2,7,10,12–16]. For the three-dimensional system, Archer and Wilding [7] used the grand canonical Monte Carlo simulation for studying the structure and phase behaviors in the bulk phase. They reported many inhomogeneous structures which depend on the value of amplitude: spherical and cylindrical liquidlike clusters, single and multi-liquidlike slabs, and cylindrical and spherical bubbles. However, their studies were restricted to particular amplitudes because of the great computational expenditure. Furthermore, their theoretical studies are limited to the random phase approximation (RPA), which is the simplest approximation for the long-range competing contribution. It is known that the density functional perturbation theory based on the RPA, which was used for structure and phase behaviors of competing fluids, does not overcome the low-temperature and high-density problems of studying the structure and phase behaviors of the hard-core Yukawa (HCY) fluid with attractive and repulsive interactions at interfaces. However, the general behavior of confined complex fluids, such as those undergoing microphase separation, has received very limited attention, even though the theory of simple fluids under confinement is well developed. Confinement induces new pattern morphologies, which might not appear at all in the bulk, and modifies the pattern morphologies. A few studies regarding the influence of confinement on the phase behaviors of competing systems have reported only on two-dimensional systems [6,9,12]. One of the important questions we consider is how the geometry of the pores, the size of the pores, and the competing interaction affect the structure and phase behaviors of confined competing fluids. Actually, the introduction of the surface force and the competition between fluid-surface and fluid-fluid forces lead to interesting surface-induced phase changes, since the periodic spacing of the modulated structure is commensurate with the periodicity of modulation in the particle density distribution. On the other hand, the precise nature of the phase behaviors of a

*sckim@andong.ac.kr
†shsuh@kmu.ac.kr

competing system in a slit pore, such as the vapor-cluster and the cluster-liquid transition, is not well understood. The present study aims to fill this gap.

The potential model that we consider is a simple hard-core model with a two-Yukawa tail potential of the form

$$\begin{aligned}\beta\phi(r) &= \infty, \quad r \leqslant \sigma, \\ &= -\frac{\varepsilon \exp[-z_1(r/\sigma - 1)]}{(r/\sigma)} \\ &\quad + \frac{A \exp[-z_2(r/\sigma - 1)]}{(r/\sigma)}, \quad r > \sigma, \end{aligned} \tag{1}$$

where $\beta = 1/k_B T$ is the inverse temperature and σ the particle diameter. In this model potential z_1 and z_2 are the ranges of interactions, and the amplitudes are $\varepsilon > 0$ and $A > 0$. For a fixed value of A, the amplitude ε plays a role somewhat akin to an inverse temperature. Depending on the values of the set of potential parameters z_1, z_2, A, ε, and number density ρ, the two-Yukawa fluid may exhibit various microphases in the bulk. In the theoretical approach for competing fluids, it is known that integral equations such as the Percus-Yevick (PY) and hypernetted-chain (HNC) equations fail to describe the new phase transition in the bulk [9,13]. These integral equations have the weakness that they cannot be directly applied to explain the modulated fluid structure of the two-Yukawa fluid confined in slit or spherical pores. The density functional perturbation theory has proved to be a powerful tool in the analysis of these problems and provides an accurate result for the structure and phase behaviors of the hard-core Yukawa fluids restricted to the special pores. The key point is how to approximate the free energy functional for the two-Yukawa fluid to overcome the low-temperature and high-density problems. Recently, Tang [17] and Karanikas *et al.* [18] applied the first-order contribution of the Yukawa direct-correlation function (DCF) based on the first-order mean-spherical approximation (FMSA) [17] and calculated the effect of wall-particle and particle-particle interactions on the solvation forces at interfaces. The main advantage is to use an analytic DCF expression for the long-range competing contribution [19,20]. They have shown that the density functional perturbation theory, which is based on the modified fundamental-measure theory (MFMT) [21,22] for hard spheres and the FMSA for the perturbation contribution, compares with the computer simulation for the structure of a HCY fluid at interfaces. However, their applications are restricted to only the structure of an attractive or repulsive HCY fluid, and do not address the structure and the phase behaviors of competing fluids with long-range attractive and repulsive interactions. In this work, we focus on the part of the structure and phase diagram in which the system in a slit pore still displays the vapor-cluster, cluster-liquid, and vapor-liquid transitions, and investigate how this is affected as one gets close to the stability limit of the confined liquid phase by increasing the intensity of the attractive part of the interaction. In the work presented in this paper, the density functional perturbation theory imposes the constraint that the particle density distribution may only vary in the direction perpendicular to the slit walls. Thus, the microphases [7], which have been identified in the bulk phase, are not distinguishable in all of these phases. For example, to see the microphases with cylinders the particle density distributions have to assume variations in two dimensions, whereas for spheres the particle density distributions must vary in all three dimensions. In this case, great computational expenditure is needed for calculating the particle density distributions.

The present paper is organized as follows. In Sec. II we will develop the density functional perturbation theory which is based both on the MFMT [21,22] for hard spheres and on the FMSA for the long-range competing interaction. In Sec. III, we apply it for investigating the structure and phase behaviors of a competing system confined in a slit pore. The structure and phase behaviors of competing fluids confined in a slit pore have been studied in detail. We discuss the results obtained for the microphase transition in a slit pore and the paper is closed with concluding remarks.

II. THEORY: DENSITY FUNCTIONAL PERTURBATION APPROACH

In the framework of a density functional perturbation theory [23] the grand potential $\Omega[\rho]$, which is a functional of the local density $\rho(\vec{r})$, is defined as the Legendre transform of the intrinsic (Helmholtz) free energy functional $F[\rho]$,

$$\Omega[\rho] = F[\rho] + \int d\vec{r}\,\rho(\vec{r})[u_{\text{ext}}(\vec{r}) - \mu], \tag{2}$$

where $u_{\text{ext}}(\vec{r})$ is the external potential and μ is the molecular chemical potential. Following the density functional perturbation theory, the intrinsic free energy functional $F[\rho]$ can be divided into the ideal free energy $F_{id}[\rho]$, the hard-sphere repulsion $F_{hs}[\rho]$, and the long-range contribution $F_{\text{comp}}[\rho]$ arising from the competing interactions:

$$F[\rho] = F_{id}[\rho] + F_{hs}[\rho] + F_{\text{comp}}[\rho]. \tag{3}$$

The ideal free energy contribution $F_{id}[\rho]$ is exactly expressed as

$$\beta F_{id}[\rho] = \int d\vec{r}\;\rho(\vec{r})[\ln \rho(\vec{r}) - 1], \tag{4}$$

where the de Broglie thermal wavelength $\Lambda = h/\sqrt{2\pi m k_B T}$ has been suppressed since it does not have any effect on the particle density distribution.

At equilibrium, the particle density distribution $\rho(\vec{r})$ satisfies the stationary condition $\delta\beta\Omega[\rho]/\delta\rho(\vec{r}) = 0$. Then, after some manipulations, the particle density distribution is given by

$$\rho(\vec{r}) = e^{\beta\mu} \exp\left\{-\beta u_{\text{ext}}(\vec{r}) + c_{hs}^{(1)}(\vec{r};[\rho]) + c_{\text{comp}}^{(1)}(\vec{r};[\rho])\right\}, \tag{5}$$

where $c_{hs}^{(1)}(\vec{r};[\rho])$ and $c_{\text{comp}}^{(1)}(\vec{r};[\rho])$ are the one-particle direct-correlation functions (DCFs) corresponding to the fluid in the pores, which are defined as $c_{hs}^{(1)}(\vec{r};[\rho]) = -\delta\beta F_{hs}[\rho]/\delta\rho(\vec{r})$ and $c_{\text{comp}}^{(1)}(\vec{r};[\rho]) = -\delta\beta F_{\text{comp}}[\rho]/\delta\rho(\vec{r})$. For calculating the particle density distributions, we need the expression for the excess free energy functionals $F_{hs}[\rho]$ and $F_{\text{comp}}[\rho]$ of the two-Yukawa fluid originating from the particle interactions. To approximate the free energy $F_{hs}[\rho]$ corresponding to the hard-sphere contribution, we here adopt the MFMT [21,22], which is known to be the most successful theory for a hard-sphere system based on the

Boublik-Mansoori-Carnahan-Starling-Leland (BMCSL) results [24,25],

$$F_{hs}[\rho] = \int d\vec{r}\,\Phi_{hs}[n_\alpha(\vec{r})], \tag{6}$$

where $\Phi_{hs}[n_\alpha(\vec{r})]$ is the excess free energy of a hard-sphere system per volume, $n_\alpha(\vec{r}) = \int d\vec{s}\rho(\vec{s})\omega_\alpha(|\vec{r}-\vec{s}|)$ is the system-averaged fundamental geometric measure of the particles, and $\omega_\alpha(r)$ is the weight function depending on the geometrical properties of species. Here, we did not describe the functional $\Phi_{hs}[n_\alpha(\vec{s})]$ in detail since it has been well documented elsewhere [21,22]. In this case, the one-particle DCF $c_{hs}^{(1)}(\vec{r};[\rho])$ is simply given by

$$c_{hs}^{(1)}(\vec{r};[\rho]) = -\int d\vec{s}\sum_\alpha \frac{\partial\Phi_{hs}[n_\alpha(\vec{s})]}{\partial n_\alpha(\vec{r})}\omega_\alpha(|\vec{r}-\vec{s}|). \tag{7}$$

The excess free energy functional $F_{\rm comp}[\rho]$, which corresponds to the contribution of the long-range competing interactions, can be calculated from the density functional approximation as

$$\beta F_{\rm comp}[\rho] = -\frac{1}{2}\int d\vec{r}\int d\vec{s}\, c_{\rm comp}^{(2)}(|\vec{r}-\vec{s}|;\rho)\rho(\vec{r})\rho(\vec{s}), \tag{8}$$

where $c_{\rm comp}^{(2)}(r,\rho)$ is the two-particle DCF for a uniform model fluid with a competing interaction and ρ is the bulk density of a system. It should be mentioned that Eq. (8) differs from the other approximations based on the density functional expansion of the free energy about the bulk density. For the particle density distribution in a confined system, the present theory, however, yields the same result as the other approximations based on the density functional expansion [19,20,23]. On the other hand, the advantage is that the present theory provides the expression for the excess free energy in the bulk phase, which is needed for calculating the phase diagram. We use the analytic DCF expression, $c_{\rm comp}^{(2)}(r,\rho)$, for the two-component Yukawa tails, which is known as the FMSA proposed by Tang [17]. In the FMSA [17], $c_{\rm comp}^{(2)}(r,\rho)$ becomes

$$\begin{aligned} c_{\rm comp}^{(2)}(r,\rho) &= \varepsilon\frac{\exp[-z_1(r/\sigma-1)]}{(r/\sigma)} - A\frac{\exp[-z_2(r/\sigma-1)]}{(r/\sigma)}, \\ & r>\sigma, \\ &= \varepsilon\{\exp[-z_1(r/\sigma-1)]/(r/\sigma) - Q(z_1)P(r,z_1)\} \\ &\quad -A\{\exp[-z_2(r/\sigma-1)]/(r/\sigma) - Q(z_2)P(r,z_2)\}, \\ & r\leqslant\sigma, \end{aligned} \tag{9}$$

where

$$\begin{aligned} Q(z) =& \ [S(z)+12\eta L(z)e^{-z}]^{-2}, \\ P(r,z) =& \ S^2(z)[e^{-z(r/\sigma-1)}]/(r/\sigma) + 144\eta^2L^2(z) \\ & \times[e^{z(r/\sigma-1)}]/(r/\sigma) - 12\eta[(1+2\eta)^2z^4 \\ & + \Delta(1+2\eta)z^5](r/\sigma)^3 + 12\eta[S(z)L(z)z^2 \\ & - \Delta(1+\eta/2)z^6](r/\sigma) - 24\eta[(1+2\eta)^2z^4 \\ & + \Delta(1+2\eta)z^5] + 24\eta S(z)L(z)(\sigma/r), \end{aligned} \tag{10}$$

with $S(z) = \Delta^2z^3 + 6\eta\Delta z^2 + 18\eta^2z - 12\eta(1+2\eta)$, $L(z) = (1+\eta/2)z + 1 + 2\eta$, and $\Delta = 1-\eta$. Here, ρ is the bulk density of the system and $\eta = \pi\rho\sigma^3/6$ is the packing fraction. We note that Archer *et al.* [8,10] introduced $c_{\rm comp}^{(2)}(r,\rho)$ as the perturbation potential such that

$$\begin{aligned} c_{\rm comp}^{(2)}(r,\rho) &= \varepsilon - A, \quad r\leqslant\sigma, \\ &= -\beta\phi(r), \quad r>\sigma, \end{aligned} \tag{11}$$

where $-\varepsilon + A$ is the value of $\beta\phi(r)$ at contact, i.e., at $r=\sigma^+$.

III. RESULTS AND DISCUSSION

A. Bulk phase diagram

In the present theory, the chemical potential μ and pressure P can be calculated from Eqs. (3), (4), (6), and (8). The chemical potential $\mu = (1/V)[\partial F(\rho)/\partial\rho]_{V,T}$ becomes

$$\begin{aligned} \beta\mu =& \ln\rho + \frac{(8\eta-9\eta^2+3\eta^3)}{(1-\eta)^3} - 4\pi\rho\int_0^\infty dr\, r^2c_{\rm comp}^{(2)}(r,\rho) \\ & - 2\pi\rho^2\int_0^\infty dr\, r^2\left(\frac{\partial c_{\rm comp}^{(2)}(r,\rho)}{\partial\rho}\right), \end{aligned} \tag{12}$$

where V is the volume of the system. The pressure $\beta P = \beta\rho\mu - \rho[\beta F(\rho)/N]$ becomes

$$\begin{aligned} \beta P =& \ \rho\frac{(1+\eta+\eta^2-\eta^3)}{(1-\eta)^3} - 2\pi\rho^2\int_0^\infty dr\, r^2c_{\rm comp}^{(2)}(r,\rho) \\ & - \pi\rho^3\int_0^\infty dr\, r^2\left(\frac{\partial c_{\rm comp}^{(2)}(r,\rho)}{\partial\rho}\right), \end{aligned} \tag{13}$$

where N is the number of particles. The liquid-vapor coexistence curve (the binodal) can be obtained by equating the pressure and chemical potential,

$$\mu_l = \mu_v \quad \text{and} \quad P_l = P_v, \tag{14}$$

where the subscripts v and l denote the vapor and liquid phases, respectively. In this case, the coexistence densities are given in terms of the bulk density ρ and the parameters ε and A. The liquid and vapor spinodal densities correspond to the locus $(\partial P/\partial\rho)_T = 0$ and the critical point corresponds to the maximum of the spinodal curve, i.e., $(\partial/\partial\rho)(\partial P/\partial\rho)_T = 0$.

The bulk phase diagram of the two-Yukawa fluids based on the FMSA treatment is displayed in Fig. 1 along with

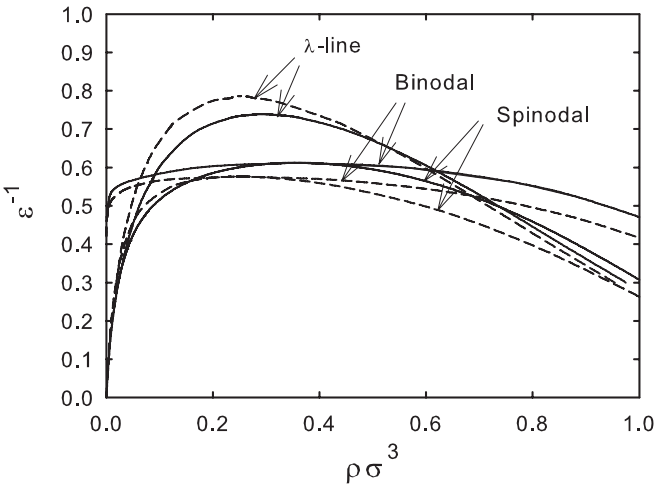

FIG. 1. Bulk phase diagram of a competing system, where $A = 0.5$, $z_1 = 1$, and $z_2 = 0.5$. The solid and dashed lines denote the present and RPA theories, respectively.

the RPA treatment, where the pair potential parameters are chosen as $A = 0.5$, $z_1 = 1.0$, and $z_2 = 0.5$ [7]. (Throughout this work, we have fixed the pair potential parameters such as $A = 0.5, z_1 = 1.0$, and $z_2 = 0.5$ since it is difficult to calculate the topology of the phase diagram in the full space of A and ϵ.). The calculated results show different phase behaviors compared with the RPA treatment; i.e., at the critical point the amplitude and density are $\varepsilon_c^{-1} = 0.6120$ and $\rho_c\sigma^3 = 0.3567$ for the present theory, whereas they are $\varepsilon_c^{-1} = 0.5761$ and $\rho_c\sigma^3 = 0.2491$ for the RPA treatment. The λ line in the bulk phase has been determined from the structure factor $S(k,\rho)$ at $k = k_c$, where k_c represents the wavelength at which the system becomes unstable, forming microphases [7]. The structure factor in the present theory is given by

$$S(k,\rho) = \frac{1}{1 - \rho\left[c_{hs}^{(2)}(k,\rho) + c_{\rm comp}^{(2)}(k,\rho)\right]}, \tag{15}$$

where $c_{hs}^{(2)}(k,\rho)$ is the two-particle DCF of hard spheres. We have calculated the two-particle DCF $c_{hs}^{(2)}(k,\rho)$ from the MFMT for hard spheres [21]. Figure 1 shows that the present theory predicts a λ line enclosing the region of the phase diagram containing the liquid-vapor critical point. Above $\varepsilon^{-1} \geqslant 0.739$, the system forms a homogeneous fluid phase. Note that the λ line in the RPA treatment meets the spinodal as a tangent. However, the FMSA does not meet this condition. It seems that the structure of the FMSA theory is very different from the RPA theory.

B. Structure and phase behaviors of the confined two-Yukawa fluids

For the hard slit pore comprising two planar surfaces, the two-Yukawa fluid interacts with the slit wall via

$$\begin{aligned} \beta u_{\rm ext}(z) &= 0, \quad \sigma/2 < z < H - \sigma/2, \\ &= \infty, \quad \text{otherwise}, \end{aligned} \tag{16}$$

where H denotes a wall separation. For the slit pore, the equilibrium particle density distribution just depends on z by a symmetric property, but not on x and y; $\rho(\vec{r}) = \rho(z)$. Thus, we define the z axis to be perpendicular to the walls. In this case, the particle density distribution, Eq. (5), becomes

$$\begin{aligned} \rho(z) = e^{\beta\mu} \exp\Bigg[& c_{hs}^{(1)}(z;[\rho]) \\ & + \int_{\sigma/2}^{H-\sigma/2} dz' c_{\rm comp}^{(2)}(|z-z'|,\rho)\rho(z') \Bigg], \\ \sigma/2 < z < H - \sigma/2 & \end{aligned} \tag{17}$$

with the planar averaged $c_{hs}^{(1)}(z;[\rho]) = 2\pi \int_0^\infty dR R c_{hs}^{(1)}(\sqrt{R^2+z^2};[\rho])$. For the numerical calculation, the trapezoidal method with $\Delta z = 0.01\sigma$ and the standard Picard iteration technique were used to calculate the particle density distribution.

The adsorption and desorption isotherms of a two-Yukawa fluid confined in a slit pore with $H = 20\sigma$ are displayed in Fig. 2(a), where $\varepsilon^{-1} = 0.55$ below the critical point $\varepsilon_c^{-1} = 0.6120$. Notice here that in the bulk phase the saturated vapor and liquid densities at $\varepsilon^{-1} = 0.55$ are $\rho_l\sigma^3 \approx 0.021$ and $\rho_v\sigma^3 \approx 0.806$, respectively. The mean density $\bar{\rho}$ inside a slit pore has been calculated as

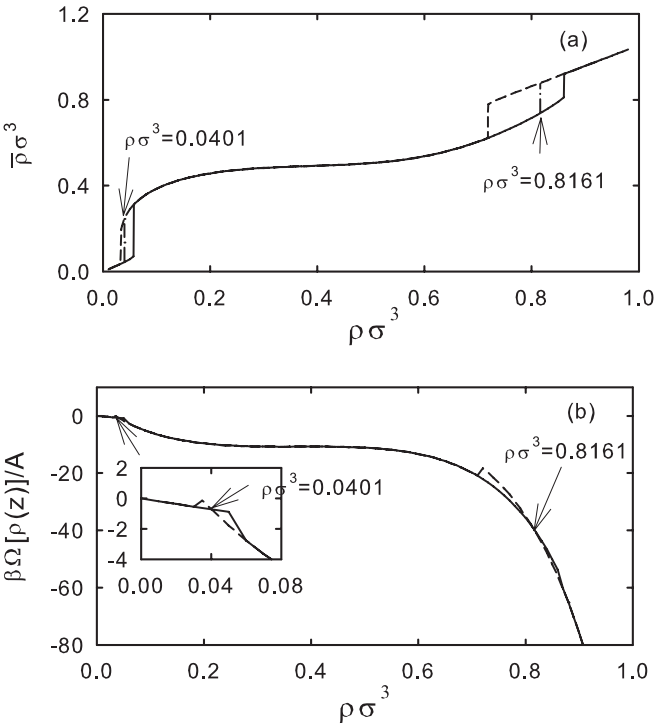

FIG. 2. (a) Adsorption (solid line) and desorption (dashed line) curves of the confined two-Yukawa fluid as a function of the bulk density $\rho\sigma^3$ ($H = 20\sigma$ and $\varepsilon^{-1} = 0.55$). The dot-dashed lines denote the equilibrium transition lines. (b) The corresponding grand potential $\beta\Omega[\rho(z)]/A$. The crosses on the curves represent the loci of equilibrium transition points.

$$\bar{\rho} = \frac{1}{(H-\sigma)} \int_{\sigma/2}^{H-\sigma/2} dz\, \rho(z), \tag{18}$$

where the mean density $\bar{\rho}$ is related to the excess adsorption Γ defined as $\Gamma = \int_{\sigma/2}^{H-\sigma/2} dz[\rho(z) - \rho] = (H-\sigma)(\bar{\rho} - \rho)$. To find the phases (vapor, cluster, and liquid) to be stable under a range of intermediate conditions, we calculated the particle density distribution twice: once starting with a high density (liquid) initial condition and once with a low density (vapor) initial condition. The adsorption curve which is plotted by the solid line in Fig. 2(a) shows that the mean density $\bar{\rho}\sigma^3$ has two sudden jumps at $\rho\sigma^3 \approx 0.058$ and 0.861, while the desorption curve denoted by the dashed line in Fig. 2(a) shows two sudden drops at $\rho\sigma^3 \approx 0.034$ and 0.719. These two solutions imply the presence of metastable states within the intervals $0.034 < \rho\sigma^3 < 0.058$ and $0.719 < \rho\sigma^3 < 0.861$. The equilibrium transition point can be determined by analyzing the dependence of the grand potential of the system in a slit pore as a function of the chemical potential $\beta\mu$ [26],

$$\beta P = -\frac{\beta\Omega[\rho(z)]}{V} = -\frac{\beta\Omega[\rho(z)]}{A(H-\sigma)}, \tag{19}$$

where $A = \int dx \int dy$ is the area of a planer interface. The corresponding grand potential $\beta\Omega[\rho(z)]$ in a slit pore is depicted in Fig. 2(b), where the grand potential becomes, from

Eqs.(2), (4), (6), and (8),

$$\frac{\beta\Omega[\rho(z)]}{A} = \int_{\sigma/2}^{H-\sigma/2} dz\,\rho(z)[\ln\rho(z)-1] + \int_{\sigma/2}^{H-\sigma/2} dz\Phi_{hs}[n_\alpha(z)] - \frac{1}{2}\int_{\sigma/2}^{H-\sigma/2} dz\,\rho(z)\int_{\sigma/2}^{H-\sigma/2} dz'\rho(z')c^{(2)}_{\rm comp}(|z-z'|;\rho_b) - \beta\mu\int_{\sigma/2}^{H-\sigma/2} dz\,\rho(z). \quad (20)$$

The cross on the curve of the grand potential versus the chemical potential represents the locus of the equilibrium transition point, i.e., the phase coexistence point. The point at which the curve crosses itself has two solutions with distinct morphologies. Note that we have plotted the grand potential as a function of the bulk density $\rho\sigma^3$ corresponding to the chemical potential for comparison with Fig. 2(a). These points are illustrated in Fig. 2(b), where the interaction points at $\rho\sigma^3 \approx 0.0401$ and 0.8161 indicate the equilibrium transition points. The vertical dash-dotted lines in Fig. 2(a) locate the average densities in a slit pore at which the thermodynamic equilibrium between two states occurs. Figure 2 indicates that there are three states and two transition points: the vapor-cluster transition at a low density and the cluster-liquid transition at a high density.

In Fig. 3 we have displayed the calculated particle density distribution $\rho(z)\sigma^3$ for the case when $\rho\sigma^3 = 0.04$, 0.40, and 0.82, where $\varepsilon^{-1} = 0.55$, $H = 20\sigma$, and 30σ. It should be mentioned that $\rho\sigma^3 = 0.4$ corresponds to the cluster phase with a large liquidlike slab, while $\rho\sigma^3 = 0.04$ and 0.82 correspond to the metastable phases near the equilibrium transition points $\rho\sigma^3 \approx 0.8161$. As can be seen from Fig. 3(a), the vapor phase shows monotonic density behaviors with

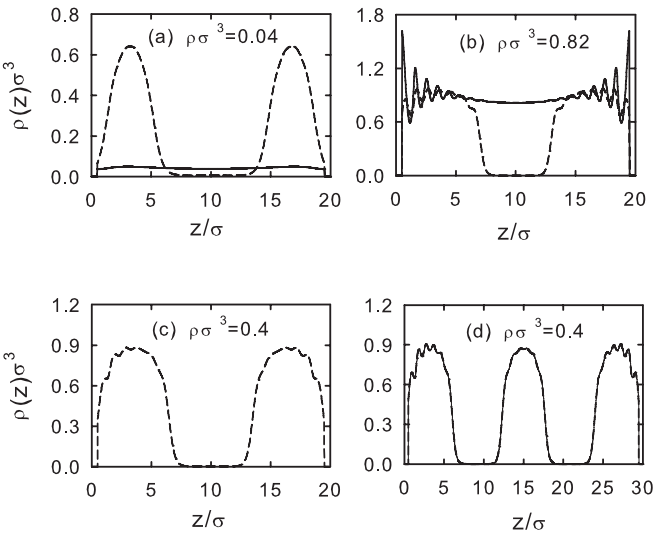

FIG. 3. Particle density distributions $\rho(z)\sigma^3$ of the confined two-Yukawa fluid ($\varepsilon^{-1} = 0.55$). (a) $\rho\sigma^3 = 0.04$ (the solid and the dashed lines denote the vapor and the cluster phases, respectively). (b) $\rho\sigma^3 = 0.82$ (the dashed and the solid lines denote the cluster and the liquid phases, respectively). (c) The cluster phase ($\rho\sigma^3 = 0.40$) at $H = 20\sigma$. (d) The cluster phase ($\rho\sigma^3 = 0.40$) at $H = 30\sigma$.

$\rho(z)\sigma^3 \approx 0.04$ except near the walls, and the mean density $\bar{\rho}\sigma^3 \approx 0.047$ is almost the same as the bulk density $\rho\sigma^3 = 0.04$. The cluster phase exhibits modulated density behavior with maximum density at $H \approx 3.2\sigma$ and 16.8σ. In this case, the mean density $\bar{\rho}\sigma^3 \approx 0.249$ is much greater than the bulk density $\rho\sigma^3 = 0.04$. However, the density at the pore middle is much smaller than the bulk density. This result indicates that the two-Yukawa fluid transforms from the initial vapor state to the cluster state with a stable liquidlike slab at $\rho\sigma^3 \approx 0.0401$. It is here noted that we consider only the morphologies in which the system forms the cluster phase parallel to the surfaces. These morphologies only require one-dimensional solutions to the particle density distribution (when the system is confined in the xy plane, the particle density distribution becomes more complicated depending on the size of a rectangular pore.) Thus, we cannot clearly distinguish the spherical shaped voids from the cylindrical shaped voids which were predicted by the computer simulation [7]. Actually, to see cylinders the particle density distributions have to assume variations in two dimensions, whereas for spheres the particle density distributions must vary in all three dimensions. In this case, we need a great computational expenditure for the particle density distributions $\rho(x,y,z)$. With increasing bulk density [see Fig. 2(a)], the vapor phase disappears. The fluid is more strongly modulated by the competition between the configurational entropic effect and the packing effect. A strong density distribution is found near the walls. At a high density $\rho\sigma^3 = 0.82$ corresponding to the metastable region for both the cluster and the liquid phases, we find a cluster with a large vaporlike void in the pore middle. The density within the cluster is close to that of the uniform liquid and the density in the voids is low, close to that of the uniform vapor, while the liquid phase exhibits a layered structure with bulk density at the pore middle due to the strong packing effect. Finally, for $\rho\sigma^3 > 0.87$ the cluster with a large vaporlike void disappears and the liquid phase only occurs at a slit pore. This result demonstrates that with increasing bulk density the confined two-Yukawa fluid transforms from a vapor to a cluster with a large liquidlike slab, and from a cluster with a large vaporlike void to a liquid. In Figs. 3(c) and 3(d) we have depicted the cluster phases with a large liquidlike slab for $H = 20\sigma$ and 30σ, where $\varepsilon^{-1} = 0.55$ and $\rho\sigma^3 = 0.4$. The cluster phase shows a double liquidlike slab for $H = 20\sigma$, whereas there is a triple liquidlike slab for $H = 30\sigma$. This implies that, as the slit width increases, the transition from a cluster with a single liquidlike slab to a cluster with a multiple liquidlike slab occurs, where the multiple liquidlike slab is formed depending on the periodicity of modulation by finite-size artifacts. This result is perhaps related to the microdomain spacing in the bulk phase, i.e., the range of the competing potential $\beta\phi(r)$. In this case a balance between the intensity of the attractive and repulsive parts of the potential yields the finite-size microphases.

The particle density distribution for the modulated structure in the bulk is displayed along with the free energy $\beta F[\rho(z)]/AH$ in Fig. 4. For the bulk phase, the cluster has periodic spacing D. The system would prefer to form the modulated structure at the equilibrium bulk spacing D, but it cannot do so if the separation between the walls H is not an integral multiple of D. The periodic spacing must be commensurate with the periodicity of modulation in the

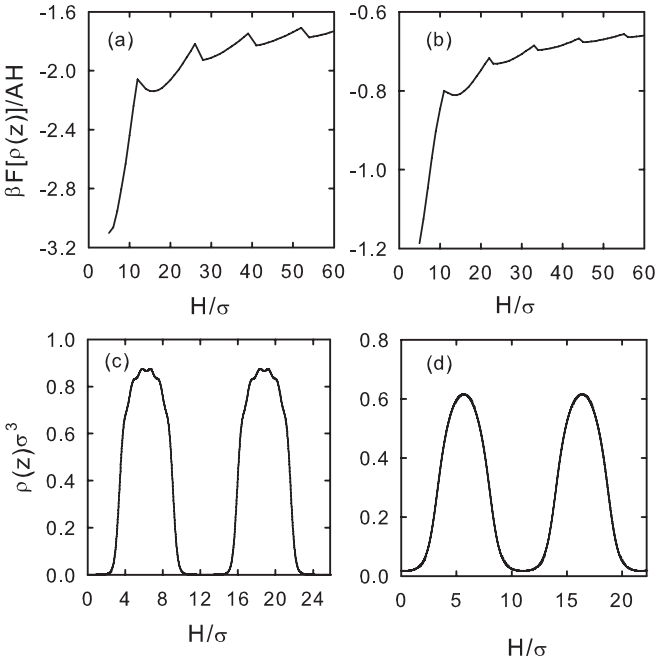

FIG. 4. (a) Helmholtz free energy for $\rho\sigma^3 = 0.4$ and $\varepsilon^{-1} = 0.55$, where the microdomain spacing is $D \approx 12.6\sigma$. (b) Helmholtz free energy for $\rho\sigma^3 = 0.25$ and $\varepsilon^{-1} = 0.65$, where the microdomain spacing is $D \approx 12.6\sigma$. (c) Modulated structure with the bulk spacing $D \approx 12.6\sigma$. (d) Modulated structure with the bulk spacing $D \approx 11.1\sigma$.

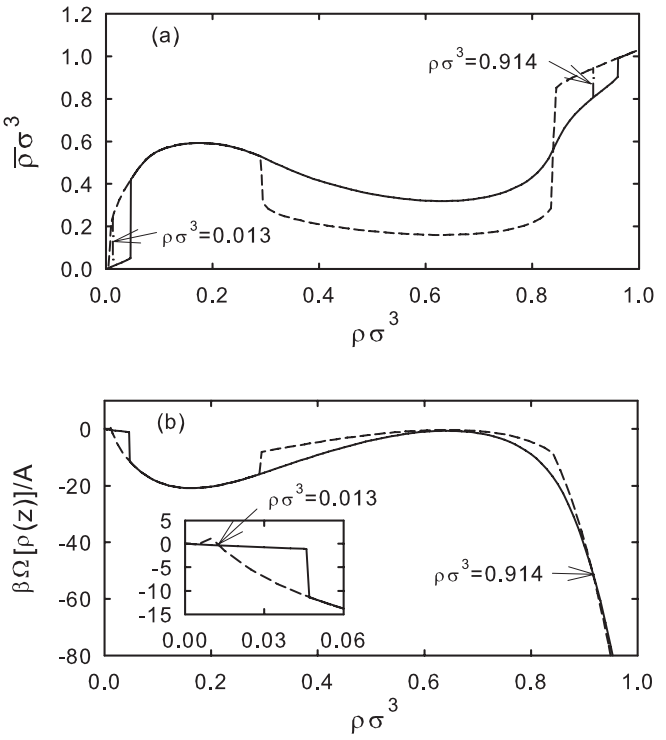

FIG. 5. The same as in Fig. 2, except for $H = 30\sigma$ and $\varepsilon^{-1} = 0.5$.

particle density distribution. The periodic spacing has been determined by the minimization of the free energy with respect to variation in H; i.e., $\partial\beta F[\rho(z)]/\partial H = 0$. For $\rho\sigma^3 = 0.4$ and $\varepsilon^{-1} = 0.55$, the microdomain spacing is $D \approx 12.6\sigma$. Notice here that the periodic spacing D depends on the potential parameter ε and the bulk density $\rho\sigma^3$; for example, the microdomain spacing is $D \approx 11.1\sigma$ for $\rho\sigma^3 = 0.25$ and $\varepsilon^{-1} = 0.65$. In this case, the particle density distribution does not exactly match as can be seen from Figs. 3(c) and 4(b). In a confined phase, we find the density oscillation near the pore wall and slightly a narrow liquidlike slab compared with that of the bulk phase.

At $\varepsilon^{-1} = 0.5$, the adsorption and desorption isotherms of a confined two-Yukawa fluid and the corresponding grand potential $\beta\Omega[\rho(z)]/A$ are presented in Fig. 5. For the adsorption curve, there are two sudden jumps at $\rho\sigma^3 \approx 0.048$ and $\rho\sigma^3 \approx 0.961$. The desorption curve shows two sudden drops at $\rho\sigma^3 \approx 0.005$ and $\rho\sigma^3 \approx 0.840$, and one sudden jump at $\rho\sigma^3 \approx 0.295$. Figure 6 shows the particle density distributions at the cluster phase and the cluster-liquid transition points. It should be mentioned that the cluster-liquid transition point as well as the periodic spacing of the cluster depends on the slit width. For example, the cluster-liquid transition point is $\rho\sigma^3 \approx 0.915$ for $H = 30\sigma$. In this case, the mean densities in a slit pore are $\bar{\rho}\sigma^3 \approx 0.812$ for the cluster phase and $\bar{\rho}\sigma^3 \approx 0.943$ for the liquid phase. For $H = 40\sigma$ the cluster-liquid transition point is $\rho\sigma^3 \approx 0.915$ and the mean densities for the cluster and liquid phase are $\bar{\rho}\sigma^3 \approx 0.714$ and $\bar{\rho}\sigma^3 \approx 0.934$, respectively. As can be seen from Figs. 5 and 6(a) for $H = 30\sigma$, we find a cluster with a single liquidlike slab [the dashed line in Fig. 6(a)] at the pore middle for the desorption curve and a cluster with a double liquidlike slab for the adsorption

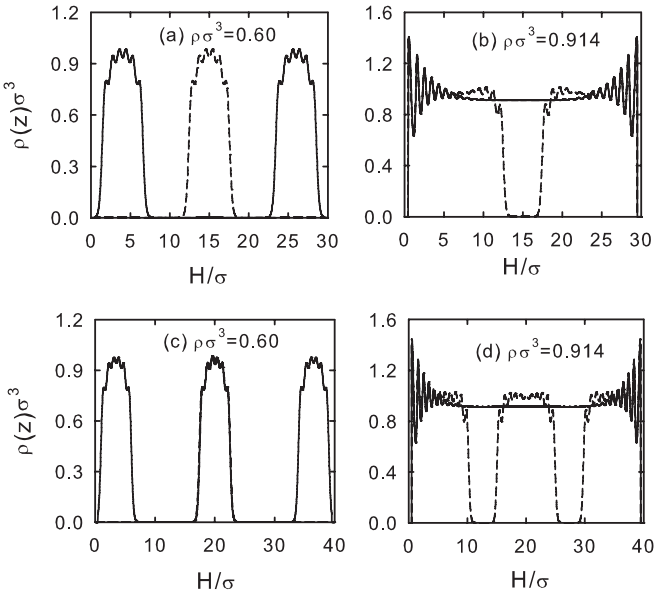

FIG. 6. Particle density distributions $\rho(z)\sigma^3$ of the confined two-Yukawa fluid ($\varepsilon^{-1} = 0.5$). (a) $H = 30\sigma$ and $\rho\sigma^2 = 0.6$ (the cluster phase). (b) The cluster and the liquid phases at the cluster-liquid transition point ($H = 30\sigma$ and $\rho\sigma^2 = 0.914$). The dashed and the solid lines denote the cluster and the liquid phases, respectively. (c) $H = 40\sigma$ and $\rho\sigma^2 = 0.6$ (the cluster phase). Notice that the single liquidlike slab at the pore middle cannot be distinguishable from the triple liquidlike slab. (d) The cluster and the liquid phases at the cluster-liquid transition point ($H = 40\sigma$ and $\rho\sigma^2 = 0.914$).

one. For $H = 40\sigma$ [Fig. 6(c)], we also find a cluster with a single liquidlike slab at the pore middle for the desorption curve, even though we cannot see a single liquidlike slab in Fig. 6(c); a single liquidlike slab with maximum density at $H = 20\sigma$ is almost the same as the case of the cluster at the pore middle among the triple liquidlike slabs of an adsorption curve. The desorption curve seems to show that there is a phase transition from a single liquidlike slab to a multi-liquidlike slab near $\rho\sigma^3 \approx 0.295$. However, the grand potential of Fig. 5(b) explains that the cluster with a triple liquidlike slab is more stable than that with a single liquidlike slab. This means that at the fixed slit pore the system does not transform from the single liquidlike slab to the multi-liquidlike slab. Figures 6(b) and 6(d) show cluster and liquid structures near the equilibrium coexistence point. The cluster exhibits a large vaporlike void depending on the periodicity of modulation and forms an array of parallel slabs, while the liquid state shows a layered structure originating from the packing effect. A comparison with Fig. 3(d) illustrates that the periodic spacing of the cluster increases with increasing intensity of an attractive part of the potential.

Figure 7(a) shows the mean density $\bar{\rho}\sigma^3$, at which the equilibrium transition occurs, as a function of the slit width H, where $\varepsilon^{-1} = 0.55$. It is here noted that the phase diagram has been obtained from the grand potential analysis in a slit pore. We find the vapor, cluster, and liquid phases with the two phase transition points as can be expected from Fig. 2. For $H > 12.7\sigma$, the phase transitions from the vapor to the

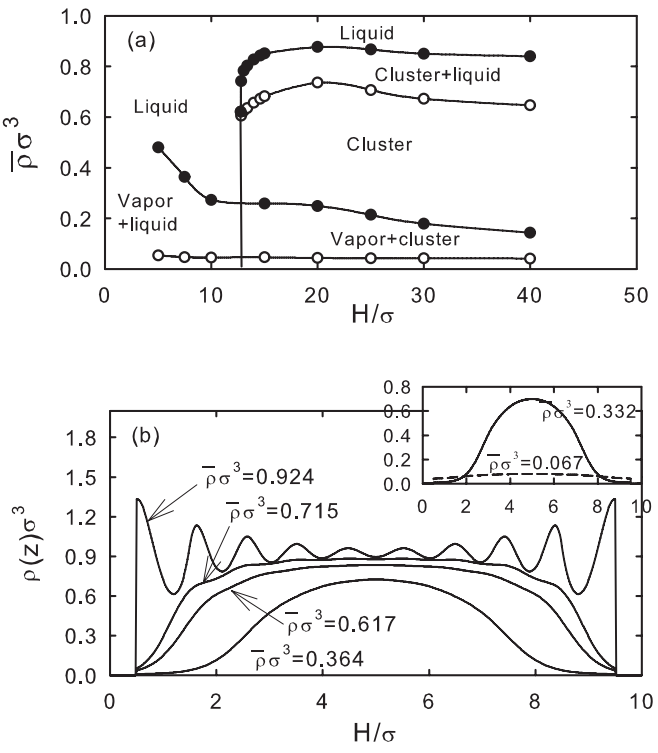

FIG. 7. (a) Phase diagram of the confined two-Yukawa fluid as a function of the slit width ($\varepsilon^{-1} = 0.55$). (b) Particle density distributions of the confined two-Yukawa fluids ($H = 10\sigma$). An inset shows the particle density distribution at the vapor-liquid transition point ($\rho\sigma^3 \approx 0.05$). The solid and the dashed lines denote the vapor and the liquid phases, respectively.

cluster and from the cluster to liquid are found. However, for the narrow slit pore ($H \leqslant 12.7\sigma$) we observe one hysteresis loop at a low density, which indicates a metastable region for both the vapor and liquid phases. Notice here that the slit width $H \approx 12.7\sigma$, at which the phase transition from the vapor to the liquid phases occurs, almost coincides with the microdomain spacing in a bulk phase. This result can be understood by considering the range of competing interactions in a slit pore. At a narrow slit pore the attractive interaction between molecules more strongly contributes to development of the particle density distribution in a slit pore compared with the repulsive interaction between molecules. Perhaps a balance between the attractive and repulsive parts of the potential yields the finite-sized microphases in a slit pore: the periodic spacing must be commensurate with the periodicity of modulation in the particle density distribution. Thus, the vapor-liquid transition at a narrow slit pore occurs as in the confined model fluids with purely attractive potential such as the Lennard-Jones and hard-core Yukawa fluids. The particle density distributions for the vapor and liquid phases are displayed in Fig. 7(b) near the phase transition point $\rho\sigma^3 \approx 0.05$, where $H = 10\sigma$. An inset shows the particle density distribution for the mean densities at which the equilibrium transition occurs. At a low density, a high density distribution is found at the pore middle due to the attractive interaction between molecules, while at a high density the packing effect is dominant. A strong density development is found at the slit walls with the usual oscillatory behavior around the bulk density in the pore middle.

At $\varepsilon^{-1} = 0.60$ near the critical point $\varepsilon^{-1} = 0.6120$, the calculated mean density $\bar{\rho}\sigma^3$ is presented in Fig. 8(a). Figure 8(b) shows the particle density distributions for different mean densities along with those of the cluster and liquid phases near the equilibrium transition point $\rho\sigma^3 \approx 0.718$, where $H = 20\sigma$. The cluster exhibits a large vaporlike void in the pore middle. The density within the cluster is close to that of the uniform liquid and the density in the voids is low, close to that of the uniform vapor. The system forms an array of parallel slabs. At high densities, the system still forms a regular array of bubbles, i.e., within the bubbles the density of particle is low, but in between the bubbles the local density is that of the liquid. One interesting thing is that, for $H \geqslant 11.8\sigma$, we only find one hysteresis loop for the adsorption and desorption curves, which indicates a metastable region for both the cluster and the liquid phases: the phase transition from a cluster with a large vaporlike void to a liquid [see the inset in Fig. 8(b)]. In this case, the repulsive interaction of the potential dominantly contributes to develop the particle density distribution in the slit pore. The vapor-liquid transition does not occur, as can be expected from Fig. 8(a). We find the cluster-liquid transition for the slit width greater than the periodic spacing of the cluster. However, the hysteresis loop becomes much narrower with decreasing slit width and eventually disappears at $H \approx 11.8\sigma$. In this case, we only find the liquid phase since the cluster is not commensurate with the periodicity of modulation in the particle density distribution. This result supports the conclusion that the confining wall effects as well as the intensity of the competing interaction exert a strong influence on the equilibrium structure and phase behaviors of the system in a slit pore.

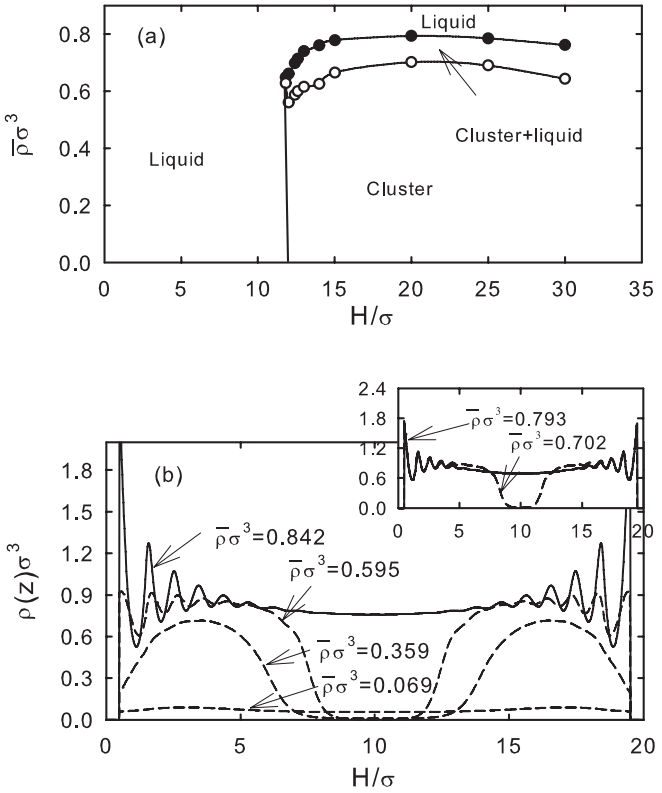

FIG. 8. (a) Phase diagram of the confined two-Yukawa fluid as a function of the slit width ($\varepsilon^{-1} = 0.60$). (b) Particle density distributions ($H = 20\sigma$). An inset shows the particle density distribution at the cluster-liquid transition point ($\rho\sigma^3 \approx 0.718$). The dashed and the solid lines denote the cluster and the liquid phases, respectively.

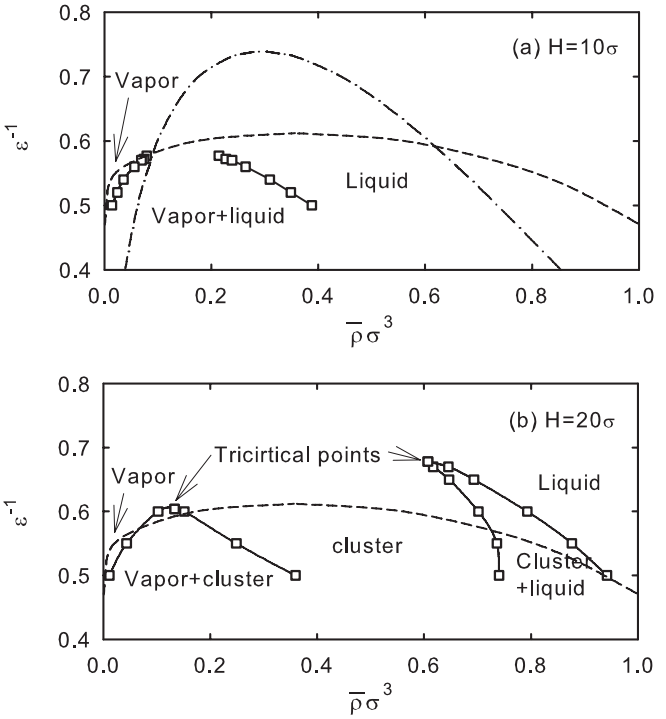

FIG. 9. Phase diagram of the confined two-Yukawa fluid. (a) $H = 10\sigma$. The dot-dashed and dashed lines denote the λline and binodal curve in the bulk phase, respectively. (b) $H = 20\sigma$.

Figure 9 depicts the phase diagrams of the two-Yukawa fluids within a slit pore with $H = 10\sigma$ and $H = 20\sigma$. At $H = 10\sigma$, as the value of ε^{-1} is increased, the first-order transition line between the vapor and the liquid phases terminates at a critical point. At the critical point in the silt pore, the amplitude and density are $\varepsilon_c^{-1} \approx 0.578$ and $\rho_c\sigma^3 \approx 0.146$, respectively. Notice here that, at the bulk critical point, the amplitude and density are $\varepsilon_c^{-1} = 0.6120$ and $\rho_c\sigma^3 = 0.3567$. This means that the critical point within a slit pore is shifted toward a high amplitude compared with that of the bulk one. The coexistence curves for the confined phase diagram are contained within the corresponding bulk liquid-vapor coexistence curve. The reason is that close to the critical point the correlation length increases, thus in one direction perpendicular to the walls the correlations are restricted due to the confinement, which results in weaker tendency toward phase separation. In this case, the cluster phase does not occur, as can be expected from Fig. 7, since the slit width is smaller than the periodic spacing required to form the cluster in a slit pore. At $H = 20\sigma$, as the value of ε^{-1} is increased, the coexistence lines meet at a particular value. This meeting point is the tricritical point. Above the tricritical points, the phase transition is second-order. The phase diagram exhibits two tricritical points, joined to one another by the line of the second-order transition. The low tricritical point is at $\varepsilon_{tc}^{-1} \approx 0.604$ and $\rho_{tc}\sigma^3 \approx 0.133$, and the higher density one is at $\varepsilon_{tc}^{-1} \approx 0.678$ and $\rho_{tc}\sigma^3 \approx 0.607$. The phase diagram shows that the cluster phase is more stable than the vapor one even for the higher amplitude. Before closing this section, we point out that we did not calculate the λ line corresponding to the second-order transition in a slit pore. Perhaps the cluster phase for the confined phase diagram is contained within the bulk λ line, and the λ line in a slit pore meets at two tricritical points as can be expected from the coexistence curves for the confined phase diagram [Fig. 9(b)]. This is another problem to overcome presently. On the other hand, it is expected that, in the case of a wide slit pore, the λ line is comparable with that of the bulk phase.

IV. CONCLUDING REMARKS

In this paper, we have employed the density functional perturbation theory, which is based both on the MFMT for hard spheres and on the FMSA for competing interactions, to investigate the structure and phase behaviors of competing fluids in a slit pore. The calculated results suggest that the confinement effect as well as the intensity of the competing interactions plays an important role in determining the equilibrium structure and phase behaviors in a slit pore. The cluster is commensurate with the periodicity of modulation in the particle density distribution. Therefore, the vapor-cluster and cluster-liquid transitions do not occur at a slit pore smaller than the periodic spacing of the cluster. For high amplitude, we only find one hysteresis loop for the adsorption and desorption curves, which indicates a metastable region for both the cluster and the liquid phases. In this case, only the phase transition from a cluster with a large vaporlike void to a liquid is found. The hysteresis loop becomes more narrow with increasing amplitude and eventually disappears at a particular slit width. In this case, we only find the liquid phase.

Note that Lutsko *et al*. [27] and Kim *et al*. [28] have recently shown that, for a value of the chemical potential corresponding to a stable liquid phase in the bulk system and a metastable vapor phase, fluid systems such as a Lennard-Jones fluid and a polymer chain fluid with a short-range attractive interaction in a hard spherical pore undergo a phase transition whereby the vapor is the stable phase at small volumes and the liquid is the stable phase at large volumes. This is an inverse of the expected behaviors in a canonical ensemble, where we expect a condensed phase to occur at low volume and a gas at high volume. However, we cannot find an inverse of the expected liquid-vapor transition in a slit pore, which demonstrates the surface-induced liquid-vapor transition. Here, one interesting thing is the relationship between the inverse liquid-vapor transition and the cluster-liquid transition, which depends on the repulsive interaction of the potential: the repulsive interaction of the potential reduces the inverse liquid-vapor transition in a slit pore. Thus, the vapor-cluster transition occurs prior to the vapor-liquid one as the pore size is reduced. On the other hand, in this paper we have only solved for the one-dimensional particle density distribution and phase, assuming invariance along the silt wall, which is bound to miss, for instance, spherical and cylindrical clusters that have been identified in the bulk phase. Thus, the phase diagrams derived in this paper are partially incomplete. To overcome this problem, we need the three-dimensional particle density distributions. We can estimate the evidence for the existence of the first-order phase transition between the spherical shaped and cylindrical shaped voids, which were reported by Archer and Wilding [7] through a computer simulation, from the grand potential of the competing systems in a slit pore. Furthermore, we did not calculate the λ line of the competing systems in a slit pore. This is another problem to overcome presently. It is very interesting to study formation of a droplet of the liquid phase from the metastable gas phase of two-Yukawa systems. In this case, a very weak long-range repulsive potential has a profound effect on nucleation [29]. Finally, the present theory suggests that the application of the FMSA theory for studying the phase behaviors of competing fluids should be restricted to spherical cavities [27] and to chain polymer fluids with the competing interaction in a slit pore [28]. We will investigate these problems in a near-future study.

ACKNOWLEDGMENTS

This research was supported by the Basic Science Research Program through the National Research Foundation of Korea (NRF) funded by the Ministry of Education, Science and Technology (Grant No. 2011-0021133).

[1] R. P. Sear, S.-W. Chung, G. Markovich, W. M. Gelbart, and J. R. Heath, Phys. Rev. E **59**, R6255 (1999).
[2] D. Pini, Ge Jialin, A. Parola, and L. Reatto, Chem. Phys. Lett. **327**, 209 (2000).
[3] A. Imperio and L. Reatto, J. Phys.: Condens. Matter **16**, S3769 (2004).
[4] A. Imperio and L. Reatto, J. Chem. Phys. **124**, 164712 (2006).
[5] A. Imperio, D. Pini, and L. Reatto, e-print arXiv:cond-mat/0703060.
[6] A. Imperio and L. Reatto, Phys. Rev. E **76**, 040402(R) (2007).
[7] A. J. Archer and N. B. Wilding, Phys. Rev. E **76**, 031501 (2007).
[8] A. J. Archer, D. Pini, R. Evans, and L. Reatto, J. Chem. Phys. **126**, 014104 (2007).
[9] A. J. Archer, Phys. Rev. E **78**, 031402 (2008).
[10] A. J. Archer, C. Ionescu, D. Pini, and L. Reatto, J. Phys.: Condens. Matter **20**, 415106 (2008).
[11] A. Ciach, Phys. Rev. E **78**, 061505 (2008).
[12] R. Roth, Mol. Phys. **109**, 2897 (2011).
[13] D. F. Schwanzer and G. Kahl, J. Phys.: Condens. Matter **22**, 415103 (2010); **14**, 33801 (2011).
[14] J. M. Bomont, J. L. Bretonnet, and D. Costa, J. Chem. Phys. **132**, 184508 (2010).
[15] E. Mani, E. Sanz, P. G. Bolhuis, and W. K. Kegel, J. Phys. Chem. C **114**, 7780 (2010).
[16] J. M. Kim, R. Castaneda-Priego, Y. Liu, and N. J. Wagner, J. Chem. Phys. **134**, 064904 (2011).
[17] Y. Tang and B. C.-Y. Lu, J. Chem. Phys. **99**, 9828 (1993); Y. Tang, *ibid*. **118**, 4140 (2004); **121**, 10605 (2004).
[18] S. Karanikas, J. Dzubiella, A. Moncho-Jordá, and A. A. Louis, J. Chem. Phys. **128**, 204704 (2008).
[19] F-Q. You, Y-X. Yu, and G-H. Gao, J. Phys. Chem. B **109**, 3512 (2005).
[20] E.-Y. Kim, S.-C. Kim, and B.-S. Seong, J. Chem. Phys. **135**, 034505 (2011); Fluid Phase Equilib. **308**, 90 (2011).
[21] R. Roth, R. Evans, A. Lang, and G. J. Kahl, J. Phys.: Condens. Matter **14**, 12063 (2002).
[22] Y. Yu and J. Wu, J. Chem. Phys. **117**, 10156 (2002); **118**, 3835 (2003).
[23] R. Evans, Adv. Phys. **28**, 143 (1979); C. N. Likos, Phys. Rep. **348**, 267 (2001).
[24] T. Boublik, J. Chem. Phys. **53**, 471 (1970).
[25] G. A. Mansoori, N. F. Carnahan, K. E. Starling, and T. W. Leland, J. Chem. Phys. **54**, 1523 (1971).
[26] A. Patrykiejew, O. Pizio, S. Sokolowski, and Z. Sokolowska, Phys. Rev. E **69**, 061605 (2004); P. Bryk, K. Bucior, S. Sokolowski, and G. Zukociński, J. Phys. Chem. B **109**, 2977 (2005); B. Peng and Y.-X. Yu, *ibid*. **112**, 15407 (2008).
[27] J. F. Lutsko, J. Laidet, and P. Grosfils, J. Phys.: Condens. Matter **22**, 035101 (2010).
[28] S.-C. Kim, E.-Y. Kim, and B.-S. Seong, J. Chem. Phys. **134**, 164701 (2011).
[29] A. J. Archer and R. Evans, Mol. Phys. **109**, 2711 (2011).